Archives of Biochemistry and Biophysics 483 (2009) 146–155

Contents lists available at ScienceDirect

Archives of Biochemistry and Biophysics

journal homepage: www.elsevier.com/locate/yabbi

Effect of structural modifications on the spectroscopic properties and dynamics of the excited states of peridinin

Nirmalya Chatterjee [a], Dariusz M. Niedzwiedzki [a], Kazuyoshi Aoki [b], Takayuki Kajikawa [b], Shigeo Katsumura [b], Hideki Hashimoto [c], Harry A. Frank [a,*]

[a] Department of Chemistry, University of Connecticut, 55 North Eagleville Road, Storrs, CT 06269-3060, USA
[b] Department of Chemistry, Kwansei Gakuin University, 669-1337, Hyogo, Japan
[c] Department of Physics, Osaka City University, 558-8585, Osaka, Japan

ARTICLE INFO

Article history:
Received 7 July 2008
and in revised form 7 October 2008
Available online 5 November 2008

Keywords:
Carotenoid
Fluorescence
Absorption
Ultrafast spectroscopy
Excited state

ABSTRACT

The spectroscopic properties and dynamics of the lowest excited singlet states of peridinin and two derivatives have been studied by steady-state absorption and fast-transient optical spectroscopic techniques. One derivative denoted PerOlEs, possesses a double bond and a methyl ester group instead of the r-ylidenebutenolide of peridinin. Another derivative denoted PerAcEs, is the biosynthetic precursor of peridinin and possesses a triple bond and a methyl ester group corresponding to the r-ylidenbutenolide function. Ultrafast time-resolved spectroscopic experiments in the visible and near-infrared regions were performed on the molecules and reveal the energies and regarding the structural features and interactions responsible for the unusual solvent-induced changes in the steady-state and transient absorption spectra and dynamics of dynamics of the excited electronic states. The data also provide information peridinin.

Introduction

Peridinin is a carotenoid found in abundance in the *Peridiniales* order of dinoflagellates [1–3]. It is an important component in a highly efficient light-harvesting apparatus that transfers energy to the photosynthetic reaction center for use in sustaining the growth of the organism. It is unusual in that its structure has an uncommon C_{37} carbon skeleton instead of the characteristic C_{40} system present in most carotenoids. It is also highly substituted with a number of functional groups including epoxide, hydroxide, and acetate groups on two terminal rings, and an allene moiety and a lactone ring in conjugation with a π-electron system of seven conjugated carbon–carbon double bonds (Fig. 1). Despite these structural modifications, the steady-state absorption and fluorescence spectra of peridinin are very similar to most other carotenoids. Peridinin has a strong absorption band in the visible spectral region (Fig. 2) that shifts characteristically to longer wavelength with increasing solvent polarizability [4,5]. Also, the fluorescence spectrum of peridinin is significantly red-shifted relative to its absorption band [6]. This behavior is well-explained by the existence of two disparate low-lying excited singlet states, denoted S_1 and S_2. Electronic transitions to and from S_1 and the ground state, denoted S_0, are forbidden by symmetry because both S_0 and S_1 are characterized by an A_g irreducible representation in the idealized C_{2h} point group. In contrast, electronic transitions to and from the S_2 state and the ground state, S_0, are allowed because S_2 has B_u symmetry in the same point group. The strong absorption in the visible region characteristic of all polyenes and carotenoids is attributable to an allowed $S_0 \rightarrow S_2$ ($g \rightarrow u$) transition. The energy of this transition has been shown to depend on solvent polarizability for carotenoids and polyenes due to dispersion interactions between the strong transition dipole and the solvent environment [7–12]. The energy of the $S_1 \rightarrow S_0$ ($g \rightarrow g$) transition, however, is hardly affected by solvent due to the fact that its low oscillator strength does not give rise to a significant transition dipole that can be influenced by interactions with the solvent environment [13]. The observation that most of the fluorescence emanating from peridinin originates from its low-lying S_1 state rather than the higher-lying S_2 state accounts for the large red-shift of its emission spectrum relative to its absorption band. This can be explained by assuming that the strict selection rules, which are adhered to in the idealized C_{2h} symmetry point group, are relaxed due to vibronic coupling between S_1 and S_2 in the highly substituted peridinin molecule [14].

The presence of the carbonyl functional group gives peridinin some unusual spectroscopic properties that distinguish it from unsubstituted carotenoids. These include a pronounced solvent effect on the shape of its steady-state absorption spectrum and a shortening the lifetime of the S_1 state with increasing solvent polarity [4,5,15–20]. In non-polar solvents the spectrum of the $S_0 \rightarrow S_2$ absorption transition of peridinin exhibits vibrational

* Corresponding author. Fax: +1 860 486 6558.
E-mail address: harry.frank@uconn.edu (H.A. Frank).

0003-9861/$ - see front matter © 2008 Elsevier Inc. All rights reserved.
doi:10.1016/j.abb.2008.10.035

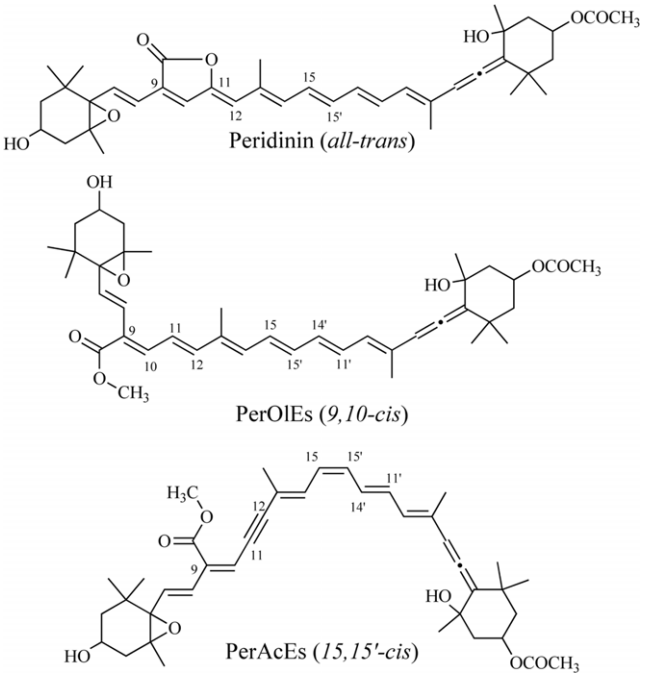

Fig. 1. Structures of peridinin and synthetic derivatives.

structure whereby peaks and shoulders associated with vibronic bands are resolved. In polar solvents, however, the vibrational structure is absent and lineshape broadens asymmetrically [4,21]. This broadening has been attributed to enhancements in conformational disorder brought about by increasing amounts of charge transfer character in S_0 [16]. Solvent induced flattening of the S_0 potential surface can result in an ensemble of conformational isomers having a wide range of effective π-electron conjugations. This would expand the distribution of $S_0 \rightarrow S_2$ transition energies and broaden the absorption spectrum [5,22].

Large changes in the transient $S_1 \rightarrow S_n$ absorption spectra of peridinin are also observed upon increasing solvent polarity. In non-polar solvents the excited state spectrum is characterized by a relatively narrow band at 510 nm reminiscent of that seen for many other carotenoids [4,21]. As the polarity of the solvent increases, the narrow band gradually disappears and is replaced by a broad absorption feature that shifts progressively to the blue [4]. The spectral broadening and shifting with increasing solvent polarity is accompanied by a decrease in the lifetime of the S_1 state [4]. This behavior was attributed to the presence of an intra-molecular charge transfer (ICT)[1] state in the vicinity of S_1 [4,16,18,21]. Precisely how the ICT state modulates the dynamics of S_1 is still unclear. Some investigators believe the S_1 and ICT are strongly mixed quantum mechanically forming a single S_1/ICT state [5,22]. Solvent polarity-induced changes of the shape of the S_1/ICT potential energy surface could then lead to the reported variations in the excited state lifetime [5,16]. Shima et al. [22] argued on the basis of two-photon spectroscopic experiments and quantum computations that a solvent polarity-induced effect on the amount of charge transfer character in the ground state of peridinin could lead to changes in its excited state lifetime. Papagiannakis et al. [23] used excitation-wavelength-dependent pump-probe, pump-dump-probe, and pump-re-pump-probe experiments on peridinin in methanol and concluded that the S_1 and ICT states are discrete entities.

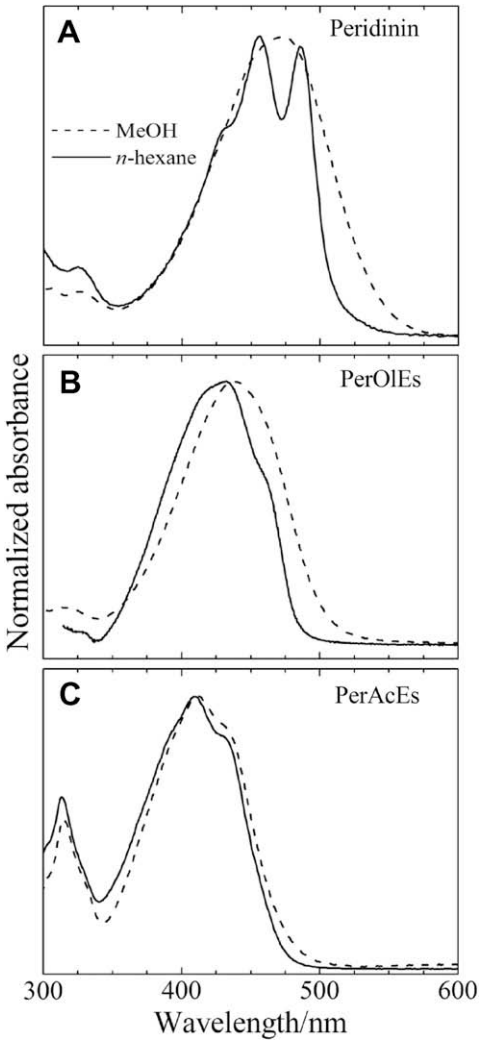

Fig. 2. Steady-state absorption spectra taken in methanol and *n*-hexane at 293 K.

Transitions from the ground state, S_0, to the ICT state are weak in both 1-photon and 2-photon absorption processes presumably due to the equilibrium excited state nuclear geometry of the ICT state being significantly different from that of the ground state. Therefore, direct spectroscopic investigations of this 'dark' ICT state are difficult to carry out, although stimulated fluorescence in the near-infrared spectral region attributable to the ICT state has been reported [17]. Quantum computations seeking to understand the nature of the electronic states of peridinin have been performed but there is little agreement among the groups [18,22]. Shima et al. [22] used MNDO-PSDCI calculations and concluded that the ICT state is simply the S_1 state with a large dipole moment derived from mixing S_2 into S_1. In contrast, Vaswani et al. [18] used time-dependent density functional theory (TD-DFT) and concluded that the ICT is a distinct electronic state whose energy is stabilized in polar solvents as previously proposed [4].

In this paper we present an investigation of the spectra and dynamics of systematically modified peridinin molecules (Fig. 1) with particular attention to how the structural modifications affect the spectroscopic behavior and kinetics of the S_1/ICT state. In order to investigate the characteristic nature of the

[1] *Abbreviations used:* ICT, intra-molecular charge transfer; TD-DFT, time-dependent density functional theory; PCP, peridinin–chlorophyll–protein; HPLC, high-performance liquid chromatograph; SVD, singular value decomposition; ESA, excited state absorption; EADS, evolution-associated difference spectra; DADS, decay-associated difference spectra.

r-ylidenebutenolide function in peridinin, two kinds of derivatives were synthesized from (−)-actinol. One derivative, denoted PerOlEs, possesses a double bond and a methyl ester group instead of r-ylidenebutenolide of peridinin. Another derivative, denoted PerAcEs, is the biosynthetic precursor of peridinin and possesses a triple bond and a methyl ester group corresponding to the r-ylidenebutenolide function. These molecules were studied to elucidate structural features responsible for the solvent-induced changes in spectra and dynamics of peridinin. The data are expected to be useful in understanding the mechanism by which peridinin carries out its light-harvesting role in the pigment-protein complexes of dinoflagellates.

Materials and methods

Sample preparation

Peridinin was extracted from the peridinin–chlorophyll–protein (PCP) complex isolated from *Amphidinium carterae* and purified as previously described [6,24]. Prior to the optical experiments, peridinin was dissolved in 4:1 (v/v) *n*-hexane:1-propanol and injected into a Millipore Waters 600E high-performance liquid chromatograph (HPLC), employing a YMC-Carotenoid C30 column and an isocratic solvent protocol. The mobile phase consisted of acetonitrile/methanol/water (87/10/3 v/v/v), and was applied for 30 min at a flow rate of 0.5 mL/min to the column equilibrated under the same conditions for 10 min prior to injection. The injection volume was 200 μL. The eluent was monitored using a Model 996 single diode-array detector, and the fraction containing peridinin was collected, dried using a gentle stream of gaseous nitrogen and stored at −20 °C until ready for use. The synthetically modified peridinin derivatives PerAcEs *Z* (15, 15′-*cis*) (hereafter referred as PerAcEs) and PerOlEs (9, 10-*cis*) were supplied as dried samples, and were similarly purified via HPLC prior to the spectroscopic measurements. Details of the synthesis will be reported elsewhere. PerAcEs was found to isomerize between the 15, 15′-*cis* (*Z*) and the *trans* (*E*) forms on standing, and is enhanced upon illumination. The *Z* isomer was found to be the more stable isomer. The stereochemistry of the *Z* isomer was confirmed by Nuclear Overhauser experiments using a 750 MHz NMR.

Spectroscopic methods

Steady-state absorption and fluorescence

The absorption spectra of peridinin, PerOlEs and PerAcEs were recorded at 293 K (room temperature, RT) in methanol and *n*-hexane using a Cary 50 UV–visible spectrometer. Absorption spectra were obtained from the samples in 4 mm (path length) × 1 cm quartz cuvettes.

Fluorescence spectroscopy was carried out using a Jobin-Yvon Horiba Fluorolog-3 model FL3-22 equipped with double monochromators having 1200 grooves/mm gratings, a Hamamatsu R928P photomultiplier tube detector, and a 450 W ozone-free Osram XBO xenon arc lamp. The fluorimeter was set to right-angle detection mode with respect to the excitation beam. The samples were placed in 1 cm (excitation path length) quartz cuvettes having a 4 mm emission path length. The emission spectra were corrected using a file generated from a 200 W quartz tungsten–halogen filament lamp. Both the emission and excitation slit widths were set at 2.5 mm corresponding to a band pass of 5 nm. The excitation wavelengths were: Peridinin, 485 nm; PerAcEs, 450 nm; PerOlEs in methanol, 480 nm; and PerOlEs in *n*-hexane, 470 nm.

Transient absorption spectroscopy

Transient absorption spectra were recorded at RT on samples adjusted to an optical density of ∼0.4 in a 2 mm (path length) quartz cuvette at the excitation wavelength. The femtosecond transient absorption spectrometer system used has been previously described [25]. The energy of the pump beam was 1 μJ/pulse in a spot size of 1.2 mm diameter which is equivalent to an intensity of $\sim 2.4 \times 10^{14}$ photons/cm^2 per pulse. The pump wavelength was chosen to be as close as possible to the 0–0 vibronic band of the $S_0 \rightarrow S_2$ of the steady-state absorption spectra of the molecules as our instrument would allow. The values were 485 nm for peridinin and 466 nm for PerOlEs and PerAcEs. The samples were constantly stirred using a magnetic micro-stirrer to prevent sample photo-degradation, and the steady-state absorption spectra were recorded before and after the transient experiments to verify sample integrity.

Surface Xplorer Pro 1.0.6 (Ultrafast Systems, LLC) software was used to correct the wavelength-dependent dispersion (chirp correction) and number of principal spectral components using the method of singular value decomposition (SVD) in the transient absorption spectra. ASUfit 3.0 software made available by Dr. Evaldas Katilius (Arizona State University) was used for global fitting calculations and for the removal of solvent response artifacts having lifetimes shorter than the pump laser pulse width.

Results

Steady-state absorption and fluorescence

The steady-state absorption spectra of peridinin, PerOlEs, and PerAcEs in methanol and *n*-hexane at RT are shown in Fig. 2. The steady-state absorption spectrum of peridinin in methanol (dashed line in Fig. 2A) is characterized by an intense, broad (FWHM 100 nm, 4600 cm^{-1}), asymmetric band at 472 nm associated with the $S_0 \rightarrow S_2$ transition. This spectrum is typical of peridinin in polar solvents where no vibronic spectral features are resolved [4]. As the solvent polarity decreases, vibronic features appear as seen in the spectrum of the molecule in *n*-hexane (solid line in Fig. 2A). The vibronic features are ∼1350 cm^{-1} apart in energy corresponding to a combination of two symmetric vibrational stretching modes with energies of 1150 cm^{-1} (σ bond) and 1600 cm^{-1} (π bond) [19].

The absorption spectrum of PerOlEs in methanol (dashed line in Fig. 2B) at RT is also broad (FWHM 87 nm, 4630 cm^{-1}) and asymmetric, but less so than peridinin. Like peridinin, PerOlEs displays no vibronically resolved features in this solvent. The maximum of the band appears at 437 nm, which is 35 nm blue-shifted compared to peridinin. In *n*-hexane, the lineshape of PerOlEs narrows slightly and a shoulder suggestive of a vibronic band appears on the long wavelength side of the spectrum (solid line in Fig. 2B). The band maximum also shifts 4 nm to the blue compared to its spectrum in methanol.

Table 1
Positions of the major vibronic bands in the steady-state absorption and fluorescence emission spectra at 293 K obtained by Gaussian deconvolution for the molecules dissolved in *n*-hexane. All values are given in nm.

	$S_0 \rightarrow S_2$ adsorption			$S_1 \rightarrow S_0$ fluorescence		
	(0–0)	(0–1)	(0–2)	(0–0)	(0–1)	(0–2)
Peridinin	486	456	429	601	656	713
PerOlEs	464	437	408	600	652	706
PerAcEs	436	409	387	558	607	664

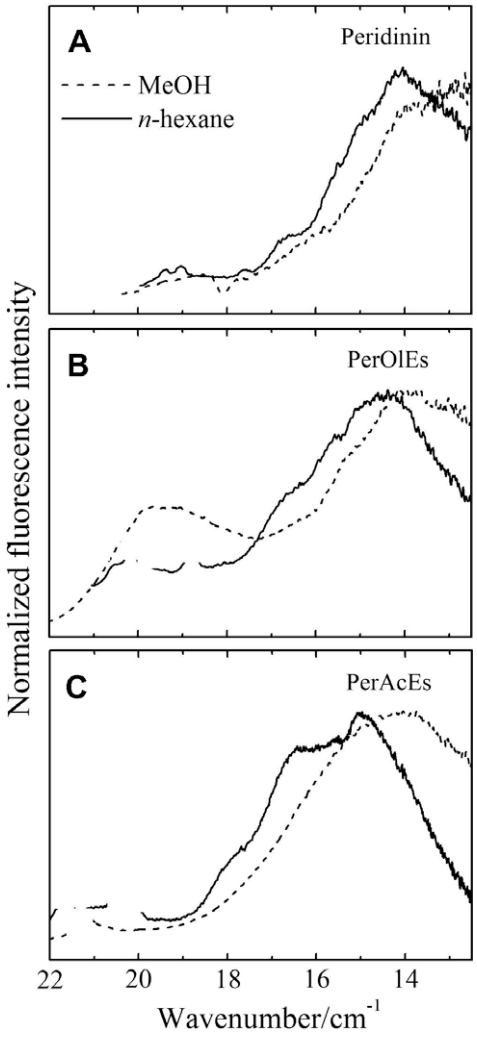

Fig. 3. Fluorescence spectra taken in methanol and *n*-hexane at 293 K. Short discontinuities in the spectra denote where Raman peaks were removed for clarity.

The absorption spectrum of PerAcEs in methanol at RT (dashed line in Fig. 2C) is also broad (FWHM 87 nm, ~5270 cm^{-1}). The maximum of the spectrum appears at ~410 nm, which is 62 nm shifted to shorter wavelength compared to peridinin in this solvent. Also, it shows a shoulder on the long wavelength side of the major absorption band suggestive of a vibronic band. In going from methanol solvent to *n*-hexane (solid lines in Fig. 2C), very little change occurs in either the width or structure of the main absorption band. This is very different from the behavior of peridinin and PerOlEs. The vibronic band positions obtained by Gaussian deconvolution absorption spectra (see below) are summarized in Table 1.

The fluorescence spectra of peridinin in methanol and *n*-hexane (Fig. 3A) display very broad bands extending into the near-infrared region beyond 700 nm (below 14,300 cm^{-1}). In *n*-hexane the spectrum displays vibronic structure. The position and shape of the fluorescence spectra from peridinin in *n*-hexane is typical of $S_1 \rightarrow S_0$ emission profiles from polyenes and other carotenoids having less than eight conjugated carbon–carbon double bonds [8,26–28]. The red-shifted, broadened fluorescence for peridinin in methanol (dashed line in Fig. 3A) most likely comes from the ICT state.

Unlike peridinin, the fluorescence spectrum of PerOlEs in methanol at RT (dashed line in Fig. 3B) shows two distinct bands at 520 nm (19,200 cm^{-1}) and 700 nm (14,300 cm^{-1}). The closeness of the first of the fluorescence bands in methanol to the $S_0 \rightarrow S_2$ absorption spectrum indicates it is due to emission from the S_2 state. The second band appearing in methanol at longer wavelength may be attributed to ICT state emission. Upon changing the solvent from methanol to *n*-hexane (solid line in Fig. 3B) the S_2 emission band shifts slightly to shorter wavelength which is consistent with the shift seen in the steady-state absorption. Also, in the non-polar solvent, *n*-hexane, the longer wavelength band narrows significantly and displays vibronic structure.

PerAcEs in methanol at RT (dashed line in Fig. 3C) shows a fluorescence spectrum similar to that of peridinin in that it is broad and appreciably red-shifted relative to its absorption spectrum. This indicates that the emission in this solvent corresponds to fluorescence from the ICT state. Changing the solvent to *n*-hexane (solid line in Fig. 3C) shifts the spectrum to higher energy, most likely due to a change in the state from which fluorescence emerges from the ICT state to the S_1 state. The band positions of the fluorescence spectra obtained by Gaussian deconvolution (see below) are summarized in Table 1.

Transient absorption in the visible region

Transient absorption spectra at various delay times are shown in Fig. 4 for peridinin, PerOlEs and PerAcEs at RT in methanol and *n*-hexane. For all the molecules, excitation results in a rapid build-up of excited state absorption (ESA) bands that then subsequently decay in tens of picoseconds back to the ground state.

For peridinin in methanol (Fig. 4A), the excited state spectra taken at various time delays are very broad with some variability in peak positions, but with an overall shape consisting of a major feature at ~600 nm and a shoulder at ~535 nm. This lineshape has been attributed to absorption from the S_1/ICT state to a higher S_n state [4,21].

Unlike peridinin, PerOlEs in methanol (Fig. 4B) shows better resolved ESA that result in two distinct bands with peaks at 504 nm and 625 nm. The band at 504 nm is diminished in intensity due to overlap with the negative band bleaching from the steady-state absorption. In the 200 fs trace, the 625 nm band is more intense by a factor of ~2 than the 504 nm band. The 504 nm band is typical of $S_1 \rightarrow S_n$ transient absorption spectra of carotenoids [4,21,29,30]. The 625 nm band is most likely as associated with absorption from the ICT state to S_n.

PerAcEs in methanol (Fig. 4C) also shows two broad, distinct bands peaking at 520 nm and 630 nm. The band at 520 nm builds up earlier than the band at 630 nm suggesting that one may be evolving from the other. The first of these bands is similar to what one would expect from $S_1 \rightarrow S_n$ ESA [4,21,29,30] and is much stronger than the second band. This is different from peridinin and PerOlEs and may be due to the fact that the $S_1 \rightarrow S_n$ band of PerAcEs is more red-shifted relative to the negative signal associated with the steady-state absorption bleaching. This would result in higher observed amplitude of the $S_1 \rightarrow S_n$ signal for PerAcEs, compared to the other molecules. Similar to that observed for PerOlEs, the second band at 630 nm may be associated with an ICT $\rightarrow S_n$ transition.

The excited state spectrum of peridinin in *n*-hexane (Fig. 4D) is much narrower than in methanol, and two primary bands are seen. The spectrum taken at 200 fs (dashed line in Fig. 4D) displays a very large band at 520 nm with a sweeping lineshape that extends to nearly 700 nm. At 5 ps (dark solid line in Fig. 4D) this band narrows and shifts slightly toward the blue to 516 nm, and another clearly noticeable, but less intense band builds up at 656 nm. In addition, a minor band occurs at 602 nm. The narrowing of this band that occurs between 200 fs and 5 ps has been attributed to vibrational cooling in the S_1 state [31,32].

The excited state absorption bands of PerOlEs in *n*-hexane (Fig. 4E) are sharper than those observed for the molecule dis-

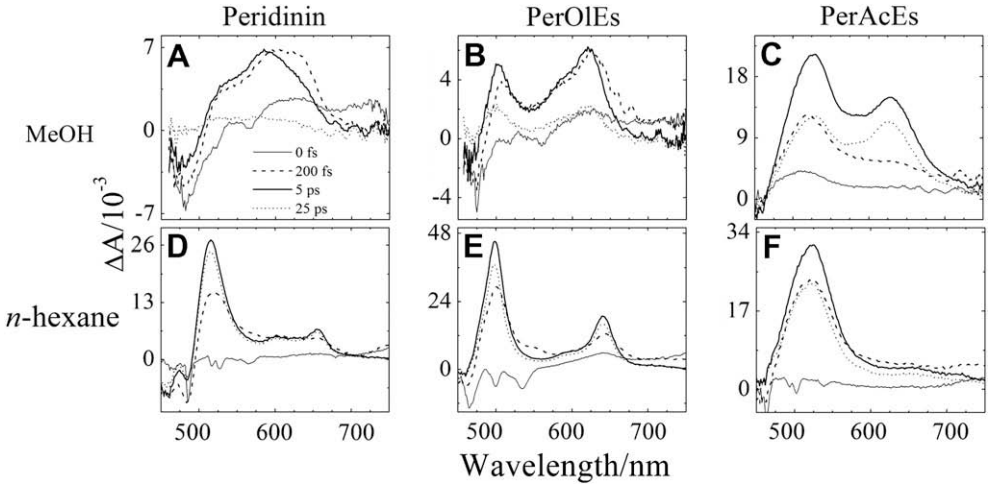

Fig. 4. Transient absorption spectra taken at different time delays in methanol and *n*-hexane at 293 K.

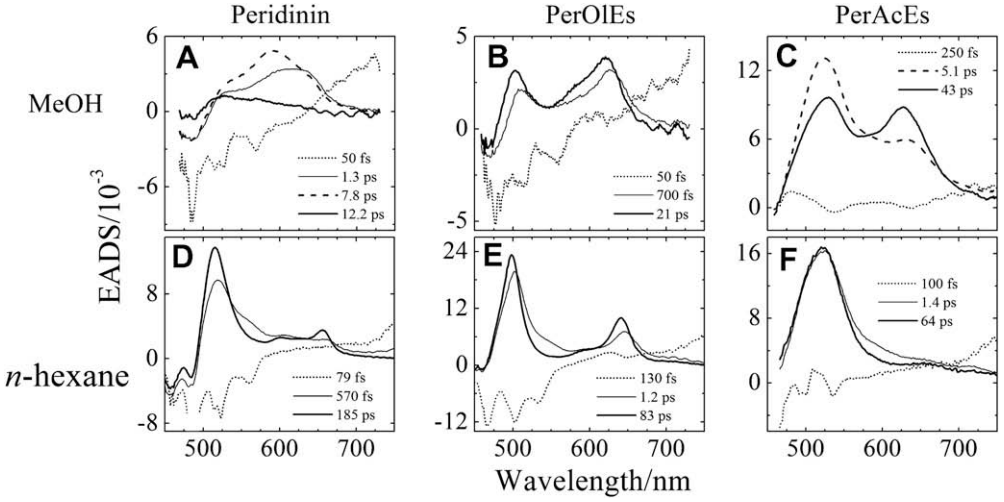

Fig. 5. Evolution associated difference spectra (EADS) obtained from global fitting the transient absorption datasets.

solved in methanol (Fig. 4B). This is similar to the behavior of peridinin (Fig. 4A and D). Also, like peridinin in *n*-hexane, two main bands are observed, a large one at 500 nm and a smaller one at 640 nm. Both features narrow as time elapses from 200 fs (dashed line in Fig. 4E) to 5 ps (dark solid line in Fig. 4E) suggestive of vibrational cooling.

In the transient absorption spectrum of PerAcEs in *n*-hexane (Fig. 4F), a major feature between 500 and 525 nm is observed, but the long wavelength band observed in methanol (Fig. 4C) is almost completely absent, and in its place is a very weak band at 660 nm.

Global analysis

The transient data represent a composite of spectral transitions associated with different states of the molecule. Each state has distinct populating and depopulating rates corresponding to different lifetimes and time-dependent concentrations. After correcting the data for wavelength-dependent dispersion and synchronizing the value of time zero across the spectral band, the number of principal spectral components in the transient spectral data set was computed using the SVD method [33]. This was used as a starting point in the global analysis. A satisfactory fit to the data was determined from a consideration of the results of a chi square (χ^2) test and minimization of the residuals [34,35].

Fig. 5 shows the global fits obtained using a sequential model with non-branching, unidirectional, multi-exponential functions associated with systematically increasing lifetimes. The resulting kinetic components obtained in this manner are termed evolution-associated difference spectra (EADS). EADS provide a visualization of the spectral characteristics of the excited states as one evolves into another [34]. A second global fitting model invoking parallel, non-interacting, decay pathways for simultaneously populated excited states was also used. The lineshapes obtained using this model are shown in Fig. 6 and are termed decay-associated difference spectra (DADS). These profiles are simply plots of the pre-exponential factors obtained after fitting the datasets to a mathematical sum of exponential kinetic terms [33,34].

Discussion

The structures of PerOlEs and PerAcEs provide a valuable opportunity to explore the molecular features that give rise to the unique spectral properties of peridinin. In going from peridinin to PerOlEs to PerAcEs the steady-state absorption spectra shift to shorter wavelength by 35 nm and 62 nm, respectively. This increase in the transition energy is due to a decrease in the effective π-electron conjugation lengths for PerOlEs and PerAcEs compared to peridinin. The reason for this effect is not obvious from the struc-

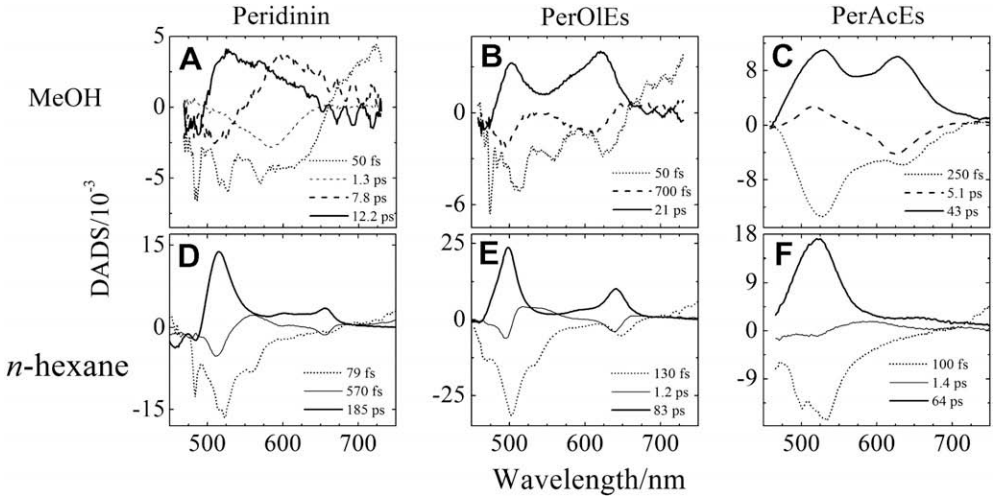

Fig. 6. Decay-associated difference spectra (DADS) obtained from global fitting the transient absorption datasets.

tures shown in Fig. 1 which appear to depict similar extents of conjugation for all the molecules. However, the absence of a closed lactone ring in PerOlEs provides the opportunity for the carbonyl to twist out of the plane of the extended conjugated polyene system of double bonds, which would decrease the effective extent of π-electron conjugation in PerOlEs compared to peridinin. For PerAcEs, the presence of the high order triple bond at the C11–C12 position introduces further shortening of the effective conjugation length compared to peridinin and PerOlEs, and leads to an additional blue shift of the absorption spectrum.

The absorption spectra of peridinin and PerOlEs broaden when the solvent is changed from non-polar to polar (Fig. 2A and B). The broadening is most pronounced and asymmetric for peridinin. This has been attributed to the charge transfer character of the ground state and the stabilization the negative charge on the carbonyl oxygen in polar solvents [21]. Charge transfer character in the ground state is thought to induce both conformational disorder and spectral broadening [5,16,19,22]. A similar argument may be made for PerOlEs and other carbonyl-containing carotenoids [16,19]. However, PerAcEs is hardly affected by solvent polarity (Fig. 2C) indicating that conformational disorder which would lead to spectral broadening is not induced by polar solvent for this molecule. The structure of PerAcEs given in Fig. 1 suggests why this may be the case. The rigid triple bond joining the C11–C12 carbons in PerAcEs effectively isolates the interactions between the polar solvent and the carbonyl from the extended π-electron conjugated chain. Therefore, the interactions have a significantly reduced ability to influence the bond orders of the conjugated π-electron system and lead to spectral broadening.

The fluorescence spectra of peridinin in *n*-hexane taken at RT (Fig. 3A) is consistent with an assignment to S_1 emission. The broadening and shift to lower energy of the fluorescence band in methanol is suggestive of emission from the ICT state. PerOlEs, however, shows two separate bands (Fig. 3B), one with a maximum at 520 nm (19,200 cm^{-1}) which is assigned to emission from the S_2 state, and a second one at 700 nm (14,300 cm^{-1}) which broadens and shifts to longer wavelength upon changing the solvent from *n*-hexane to methanol suggestive of a change in emission from the S_1 state to emission from the ICT state. The relative intensity of the two bands depends on the solvent which may influence the rate of decay from the S_1, ICT and S_2 excited states and therefore, the quantum yields of emission. The dual state emission observed for PerOlEs (Fig. 3B) is not unusual for carotenoids having eight or less conjugated carbon–carbon double bonds [36]. The

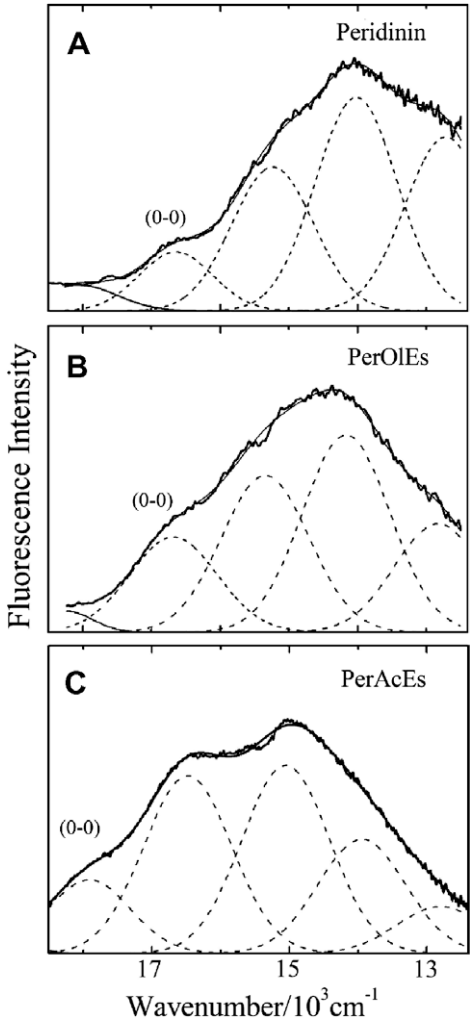

Fig. 7. Gaussian deconvolution of the fluorescence spectra taken in *n*-hexane at 293 K.

fluorescence spectrum of PerAcEs shifts to lower energy upon changing the solvent from *n*-hexane to methanol consistent with the idea that fluorescence emerges from the S_1 state in non-polar solvents and from the ICT state in polar solvents.

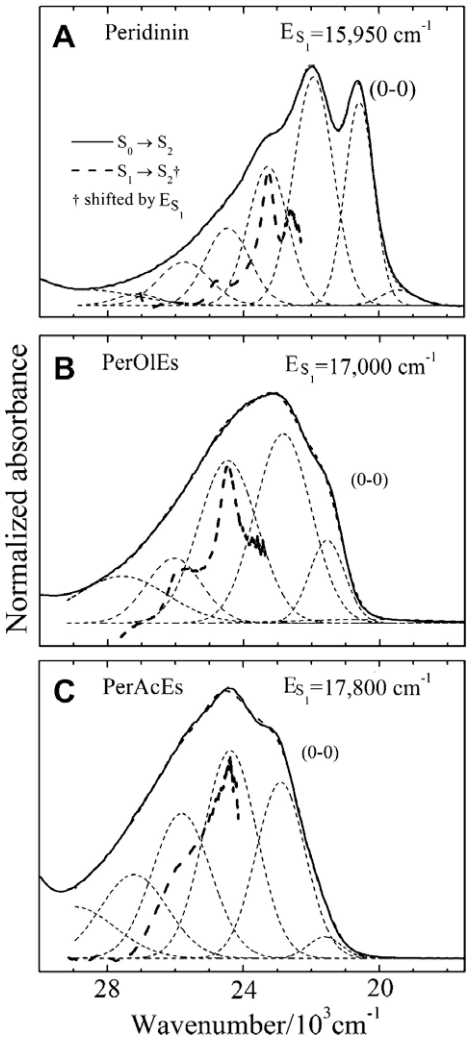

Fig. 8. S_1 energies (E_{S_1}) computed by aligning the vibronic features (thin dashed lines) of the $S_0 \rightarrow S_2$ visible absorption spectra and the $S_1 \rightarrow S_2$ transient absorption spectra (thick dashed lines) taken in the near-infrared region.

The unstructured nature of the fluorescence emission bands for the molecules in the polar solvent, methanol, precludes a detailed analysis of the underlying vibronic band structure. However, Gaussian deconvolution of the $S_1 \rightarrow S_0$ fluorescence spectra taken in the non-polar solvent, *n*-hexane, is feasible. (See Fig. 7.) The analysis reveals the positions of the (0–0) vibronic bands which approximate the energies of the S_1 state. The values are 16,600 ± 600 cm^{-1}, 16,700 ± 800 cm^{-1}, and 17,900 ± 700 cm^{-1} for peridinin, PerOlEs, and PerAcEs, respectively.

The S_1 energies may also be determined from $S_1 \rightarrow S_2$ transient absorption experiments [37]. This is done by measuring the energy of the $S_1 \rightarrow S_2$ transition in the near-infrared region using transient absorption methods and then subtracting this value from the energy of the $S_0 \rightarrow S_2$ transition obtained from steady-state absorption experiments. This is illustrated graphically in Fig. 8 where the $S_0 \rightarrow S_2$ steady-state absorption spectra of peridinin, PerOlEs and PerAcEs in *n*-hexane are shown on a wavenumber scale (solid lines). Gaussian deconvolution (thin dashed lines) reveals the vibronic bands in the spectra. The $S_1 \rightarrow S_2$ transient absorption profiles (thick dashed lines) were obtained in the near-infrared region, converted to a wavenumber scale, and then using the values from the fluorescence measurements as a first approximation, shifted horizontally along the energy axis to line up with the vibronic bands of the steady-state spectra of the individual molecules. The amount of the energy shift needed to obtain agreement between the $S_0 \rightarrow S_2$ and $S_1 \rightarrow S_2$ spectra is a measure of the S_1 energy. The values are labeled E_{S_1} in Fig. 8 and were found to be 15,950 ± 700 cm^{-1}, 17,000 ± 1000 cm^{-1}, and 17,800 ± 900 cm^{-1} for peridinin, PerOlEs, and PerAcEs, respectively. The uncertainties correspond to one-half of the full-width at half-height of the fitted Gaussian bands.

Previous studies have reported that S_1 energies of carotenoids obtained from fluorescence emission spectral lineshapes are systematically 500–800 cm^{-1} higher than those obtained from $S_1 \rightarrow S_2$ transient absorption measurements. (For a review of this topic see Ref. [21].) This discrepancy has been explained by the fact that the $S_1 \rightarrow S_2$ transient absorption technique probes allowed ($g \rightarrow u$) transitions, whereas fluorescence $S_1 \rightarrow S_0$ examines forbidden ($g \rightarrow g$) transitions. If an ensemble of twisted conformers exists in the S_1 state, which is very likely the case, not only for the molecules studied here, but for all carotenoids, fluorescence will detect emission primarily from molecules possessing deviations from idealized symmetry. On the other hand, the primary contribution to the allowed $S_1 \rightarrow S_2$ transient absorption spectrum will be from conformers in the ensemble having a high degree of symmetry. This may also explain why the vibronic features in the $S_1 \rightarrow S_2$ NIR spectra are narrower than those observed for the $S_1 \rightarrow S_0$ fluorescence or $S_0 \rightarrow S_2$ absorption spectra. A difference in S_1 energies obtained by fluorescence spectroscopy compared to $S_1 \rightarrow S_2$ transient absorption then emerges because the different techniques are examining separate subsets of conformers [21]. Taking into account this systematic difference in the experimental methods and the uncertainties in the measurements, the values obtained here from the two techniques are reasonably consistent.

We now turn to the issue of the decay pathways for excited state energy dissipation following photoexcitation. The results from a global fitting analysis of the transient datasets using a sequential (EADS) decay mechanism are shown in Fig. 5 and summarized in Table 2. In all cases the component with the shortest lifetime is associated with transitions involving the initially-populated S_2 state. The strong negative EADS amplitude below 600 nm (e.g. see Fig. 5A, B, D and E) in this component is due either to bleaching of the $S_0 \rightarrow S_2$ transition or to stimulated emission from the S_2 state. The slight rise in amplitude of the first EADS above 700 nm (Fig. 5A, B, D, E) is due to $S_2 \rightarrow S_n$ transient absorption [5,17].

For peridinin, the second EADS component (thin solid line, 1.3 ps, Fig. 5A) is similar in shape but appears at longer wavelength compared to the third EADS component (thick dashed line, 7.8 ps, Fig. 5A). These EADS components show identical negative amplitudes below 500 nm attributable to ground state bleaching. This suggests little change in ground state population occurs in this time domain. Therefore, the second EADS may be associated with

Table 2
Lifetimes of the global fitting components obtained from the transient absorption datasets of peridinin, PerOlEs and PerAcEs dissolved in methanol and *n*-hexane at 293 K.

	In methanol	In *n*-hexane
Peridinin	50 ± 5 fs	79 ± 1 fs
	1.3 ± 0.1 ps	570 ± 10 fs
	7.8 ± 0.1 ps	185 ± 1 ps
	12.2 ± 0.1 ps	
PerOlEs	50 ± 10 fs	130 ± 10 fs
	700 ± 10 fs	1.2 ± 0.1 ps
	21 ± 1 ps	83 ± 1 ps
PerAcEs	250 ± 10 fs	100 ± 10 fs
	5.1 ± 0.1 ps	1.4 ± 0.1 ps
	43 ± 1 ps	64 ± 1 ps

vibrationally hot S_1 and ICT states which equilibrate in 1.3 ps to form a composite S_1/ICT band envelope, the spectrum of which is expected to shift to the blue upon vibronic cooling. The third EADS shows a broad ESA between 500 nm and 700 nm. The broadening has been related to solvent-induced-conformational disorder of the molecule in a polar solvent. This component is associated with the lifetime of the S_1/ICT state which decays in 7.8 ps [4,5,17]. The fourth and last EADS component of peridinin (thick solid line, 12.2 ps, Fig. 5A) displays a single weak band at 505 nm. This band has been assigned to a transition from a "pure" S_1-like state of peridinin based on an analysis of dispersed pump-probe, pump-dump-probe and pump-re-pump-probe transient absorption experiments carried out by Papagiannakis et al. [23]. However, the lifetime of this component does not agree with that obtained in the non-polar solvent *n*-hexane (185 ps, see below). This may be due to population depletion of the S_1 state into the closely spaced ICT state.

Global fitting of the transient dataset from PerOlEs in methanol requires three EADS components for a satisfactory fit (Fig. 5B). Similar to peridinin, the first EADS component (dotted line, 50 fs, Fig. 5B) is due primarily to ground state bleaching, stimulated emission or ESA (at longer wavelength) involving the S_2 state. The second and third EADS components show two major bands near 504 nm and 625 nm suggestive of $S_1 \rightarrow S_n$ and ICT $\rightarrow S_n$ transitions. The 625 nm band narrows and shifts to the blue as the second EADS component evolves into the third component, indicative of vibronic cooling as described above for peridinin.

Global fitting of the transient dataset from PerAcEs in methanol also required three EADS components for a satisfactory fit (Fig. 5C). The initial EADS (dotted line, 250 fs, Fig. 5C) is associated with the decay of the S_2 state. As observed for PerOlEs, the second and third EADS lineshapes possess two strong bands at 520 nm and 630 nm suggestive of $S_1 \rightarrow S_n$ and ICT $\rightarrow S_n$ transitions. The build-up in amplitude of the 630 band at the expense of the 520 band in going from the second to the third EADS suggest transfer of population from the S_1 state to the ICT state in 5.1 ps. The subsequent decay of both signals back to the ground state in 43 ps suggests that the S_1 and ICT states are strongly coupled.

Global fitting of the transient absorption data of peridinin in the non-polar solvent, *n*-hexane, using the sequential model gave three EADS components (Fig. 5D). The fastest component (dotted line, 79 fs, Fig. 5D) is due primarily to stimulated emission from the S_2 state. The second component has a very broad lineshape (thin solid line, 570 fs, Fig. 5D) that can be attributed to ESA from a vibrationally hot S_1 state. This state decays into another state associated with the third and final EADS component (thick solid line, 185 ps, Fig. 5D) whose major band at 516 nm narrows as a result of vibrational cooling. The longest wavelength peak in the third EADS may be assigned to a transition between the excited S_1 and S_3 states, where S_3 is the state into which absorption from the ground state, S_0, is strongly allowed for *cis* isomers. This is rationalized as follows: The transition energy of the transient absorption peak appearing at 656 nm is 15,200 cm^{-1}. If this amount of energy is added to the S_1 energy of 15,950 cm^{-1} determined from the data given in Fig. 8, a value of 31,150 cm^{-1} for the $S_0 \rightarrow S_3$ transition energy is obtained. This agrees reasonably well with the energy of 30,800 ± 500 cm^{-1} corresponding to the $S_0 \rightarrow S_3$ *cis* peak transition appearing at 325 ± 5 nm in the steady-state absorption spectrum of peridinin (solid line, Fig. 2A). An important point to note is that for peridinin in this solvent, there is no evidence for any steady-state or transient absorption transitions involving the ICT state. Thus, the S_1 lifetime of peridinin is longer in *n*-hexane compared to that in methanol due to the absence of the ICT state providing a route for excited state deactivation.

Similar to peridinin, global fitting of the transient dataset from PerOlEs in *n*-hexane required three EADS components (Fig. 5E) for a good fit. For PerOlEs the lifetimes of the components are 130 fs for the transitions involving the S_2 state (dotted line, Fig. 5E), 1.2 ps for the vibrationally hot S_1 state (thin solid line, Fig. 5E) and 83 ps for the vibronically relaxed S_1 state (thick solid line). (See also Table 2.) Applying the same reasoning used for peridinin, the small band at 640 nm may be assigned to a $S_1 \rightarrow S_3$ transient *cis* peak transition, and once again in *n*-hexane, there is no evidence for any transition involving the ICT state in PerOlEs.

PerAcEs in *n*-hexane shows three EADS components (Fig. 5F), the fastest of which (dotted line, 100 fs, Fig. 5F) can be assigned by analogy with the other molecules to stimulated emission to form the S_2 state accompanied by an only partially evident (above 700 nm) $S_2 \rightarrow S_n$ transient absorption band. The second EADS component (thin solid line, 1.4 ps, Fig. 5F) is a broadened version of the final EADS component (thick solid line, 64 ps, Fig. 5F) suggestive of vibronic cooling.

Global fitting of the transient absorption spectral datasets according to a parallel (DADS) decay model was used in an attempt to gain more insight into the mechanism of excited state deactivation of the molecules. Fig. 6A shows the four DADS components required to fit the transient data from peridinin using a parallel model. The negative amplitude in the first component (dotted line, 50 fs, Fig. 6A) below 550 nm is due to the stimulated emission from the S_2 state. The positive amplitude above 700 nm is due to transient $S_2 \rightarrow S_n$ absorption. The S_2 state is depopulated in 50 fs to form a combined S_1/ICT state that equilibrates in 1.3 ps. This equilibration time is represented by the second DADS component (thin dashed line, 1.3 ps, Fig. 6A) having negative amplitude and a band centered at 580 nm. The equilibrated S_1/ICT state then decays in 7.8 ps to the ground state as evidenced by the third DADS component (thick dashed line, 7.8 ps, Fig. 6A). The final DADS (solid line, 12.2 ps, Fig. 6A) is identical to the one observed in the EADS (Fig. 5A) and, as mentioned above, may be a kinetic component associated with a pure $S_1 \rightarrow S_n$ transition.

Fig. 6B shows the three DADS components required for a good fit to the dataset for PerOlEs in methanol. As discussed above for the EADS analysis, the fastest component (dotted line, 50 fs, Fig. 6B) is similar to the one seen for peridinin (dotted line, 50 fs, Fig. 6A) and is associated primarily with stimulated emission from the S_2 state. The second DADS component for PerOlEs is associated with a vibronically hot ICT state transition (dashed line, 700 fs, Fig. 6B) that gives way to the third and final DADS component (solid line, 21 ps, Fig. 6B) which displays a combination of a typical $S_1 \rightarrow S_n$ transition at shorter wavelength (500 nm) and an ICT excited state transition at longer wavelength (620 nm) that decay together in 21 ps suggestive of an equilibration between the two.

Fig. 6C shows three DADS components are required for a good fit to the dataset from PerAcEs. The first component (dotted line, 250 fs, Fig. 6C) shows a negative band at 525 nm signifying a very rapid buildup of an ESA. The second component (dashed line, 5.1 ps, Fig. 6C) can be attributed to a process that transfers population from the 525 nm band (positive amplitude) to the 630 nm band (negative amplitude). If the 525 nm band is assigned to the $S_1 \rightarrow S_n$ transition, which is entirely reasonable given that is where the transition appears for the molecule in *n*-hexane (Fig. 6F), and the 630 nm band is assigned to the ICT $\rightarrow S_n$ transition, the 5.1 ps component then most likely represents the rate of establishing equilibrium between the S_1 and ICT states. This is slower than the 1.3 ps and 700 fs equilibration times for peridinin and PerOlEs, respectively, most likely due to a higher activation barrier for populating the ICT state from S_1. Of course, once equilibrium is established between the ICT and S_1 states, the two bands will decay simultaneously (in 43 ps) to the ground state as observed.

Fig. 6D shows the three DADS components required to fit the transient absorption dataset obtained for peridinin in *n*-hexane. The fastest component (dotted line, 79 fs, Fig. 6D) is the component

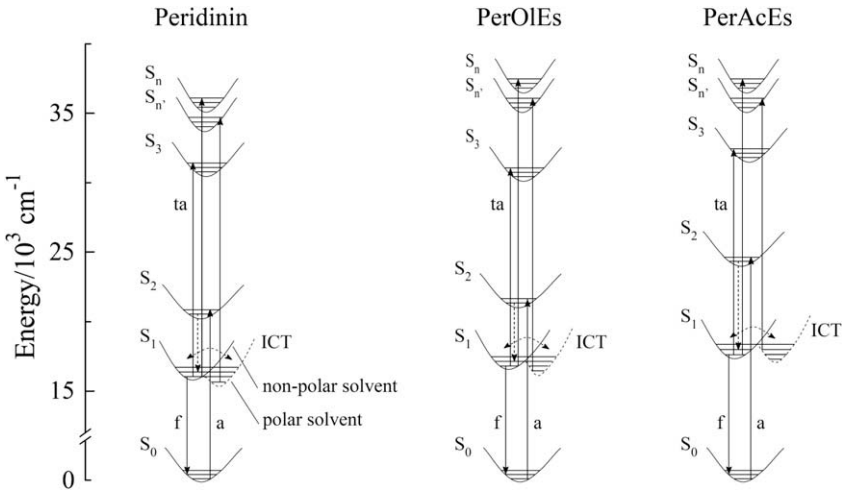

Fig. 9. Potential energy level diagrams and associated spectroscopic transitions for the molecules in polar and non-polar solvents: ta, transient absorption; f, fluorescence; a, absorption. The solid lines correspond to radiative transitions, and the dashed lines correspond to non-radiative processes.

associated with the stimulated emission from the S_2 state. The second component (thin solid line, 570 fs, Fig. 6D) is consistent with the build-up of vibrationally hot S_1 states from which $S_1 \rightarrow S_n$ and $S_3 \rightarrow S_n$ transitions occur as discussed above. This component decays into a third component (thick solid line, 185 ps, Fig. 6D) which is attributed to the same $S_1 \rightarrow S_n$ and $S_3 \rightarrow S_n$ transitions, but in this case are vibronically relaxed.

Fig. 6E shows the three DADS components required for a good fit to the transient absorption dataset for PerOlEs in *n*-hexane. The same rationale used for peridinin in *n*-hexane applies for other molecules. The fastest component (dotted line, 130 fs, Fig. 6E) is associated with the stimulated emission from the S_2 state. The second component (thin solid line, 1.2 ps, Fig. 6E) which is almost entirely negative, is attributed with the build-up of vibrationally hot S_1 states from which $S_1 \rightarrow S_n$ and $S_1 \rightarrow S_3$ transitions occur. The second component decays into a positive amplitude third component (thick solid line, 83 ps, Fig. 6E) which contains bands attributed to vibronically relaxed $S_1 \rightarrow S_n$ and $S_1 \rightarrow S_3$ transitions.

Fig. 6F shows the three DADS components needed to obtain a good fit for PerAcEs in the non-polar solvent, *n*-hexane. The fast component (dotted line, 100 fs, Fig. 6F) is almost entirely negative except above 700 nm where an $S_2 \rightarrow S_n$ transition occurs. This is similar to that seen for the first DADS components of peridinin and PerOlEs (Fig. 6D and E). The second DADS component for PerAcEs has both positive and negative bands that give way to a third DADS that is entirely positive with bands at 525 and 660 nm. The weak band at 660 nm is most likely a transient *cis* peak, analogous to that seen for the other molecules.

It is important to note that despite the S_1 energies of the molecules increasing in the order, peridinin < PerOlEs < PerAcEs, the S_1 lifetimes of the molecules in *n*-hexane decrease from 185 ps to 83 ps to 64 ps; i.e. instead of the S_1 lifetime getting longer as expected from the fact that the effective conjugation length gets shorter for the molecules in that order, the lifetime of PerOlEs (83 ps) is approximately half of that of peridinin (185 ps), and PerAcEs is even shorter (64 ps). This behavior is reminiscent of that observed from various apo-β-carotenals [38–40]. As the conjugated chain length of the apo-β-carotenals decreases from $N = 10$ to 8 the S_1 lifetime gets longer. However, at the point where one gets to 15′-apo-β-caroten-15′-al (retinal, $N = 6$), the trend is no longer followed. Retinal has much shorter lifetime (31 ± 11 ps in *n*-hexane [41], 34 ps in cyclohexane [42], and 21 ps in 1-butanol [42]) than expected on the basis of extrapolation from the longer apo-β-carotenals. This may be explained by the presence of a low-lying $n\pi^*$ state [42] which may also be playing a role in the mechanism of deactivation of the peridinin derivatives. Alternatively, PerOlEs and PerAcEs exist most stably as *cis* isomers (Fig. 1). Quantum computations on conjugated polyenes indicate that the electronic coupling terms are significantly higher for *cis* isomers compared to *trans* isomers, and when combined with the Franck–Condon factors, predict significantly faster internal conversion rates for the *cis* molecules. The computations suggest that electronic effects more than offset the decrease in coupling efficiencies associated with the higher system origin energies. This would account for the observed shorter lifetimes for *cis* isomers compared to *trans* isomers [43].

Fig. 9 summarizes the affect of structural modifications to peridinin on the excited state energies and corresponding shapes of the potential energy surfaces of the derivative molecules. The figure also shows the various spectroscopic transitions associated with the molecules and indicates that the barrier for the transfer of population from the initially-populated S_1 state to the ICT state in polar solvent is affected by the structural modifications. The change in barrier height alters the equilibration time between the S_1 and ICT states and supports the view that these two states are distinct and associated with different molecular conformations having horizontally offset potential energy surface minima.

Acknowledgments

The authors wish to thank Profs. Tomáš Polívka and Robert Birge for several useful discussions. This work has been supported in the laboratory of HAF by a grant from the National Institutes of Health (GM-30353) and by the University of Connecticut Research Foundation.

References

[1] J.E. Johansen, W.A. Svec, S. Liaaen-Jensen, F.T. Haxo, Phytochem. 12 (1974) 2261.
[2] T.W. Goodwin, The Biochemistry of the Carotenoids, Chapman & Hall, London, 1980.
[3] J.A. Haugan, T. Aakermann, S. Liaaen-Jensen, in: G. Britton, S. Liaaen-Jensen, H. Pfander (Eds.), Carotenoids, Birkhäuser Verlag, Basel, 1995, pp. 222–226.
[4] J.A. Bautista, R.E. Connors, B.B. Raju, R.G. Hiller, F.P. Sharples, D. Gosztola, M.R. Wasielewski, H.A. Frank, J. Phys. Chem. B 103 (1999) 8751–8758.
[5] D. Zigmantas, R.G. Hiller, A. Yartsev, V. Sundström, T. Polivka, J. Phys. Chem. B 107 (2003) 5339–5348.
[6] J.A. Bautista, R.G. Hiller, F.P. Sharples, D. Gosztola, M. Wasielewski, H.A. Frank, J. Phys. Chem. A 103 (1999) 2267–2273.

[7] S. Basu, Adv. Quantum Chem. 1 (1964) 145–169.
[8] B. Hudson, B. Kohler, Ann. Rev. Phys. Chem. 25 (1974) 437–460.
[9] P.O. Andersson, T. Gillbro, L. Ferguson, R.J. Cogdell, Curr. Res. Photosynth., Proc. Int. Conf. Photosynth., 8th 2 (1990) 117–120.
[10] P.O. Andersson, T. Gillbro, L. Ferguson, R.J. Cogdell, Photochem. Photobiol. 54 (1991) 353–360.
[11] P.O. Andersson, T. Gillbro, J. Chem. Phys. 103 (1995) 2509–2519.
[12] H.A. Frank, Arch. Biochem. Biophys. 385 (2001) 53–60.
[13] B.S. Hudson, B.E. Kohler, K. Schulten, in: E.D. Lim (Ed.), Excited States, Academic Press, New York, 1982, pp. 1–95.
[14] K. Schulten, M. Karplus, Chem. Phys. Lett. 14 (1972) 305–309.
[15] S. Akimoto, S. Takaichi, T. Ogata, Y. Nishimura, I. Yamazaki, M. Mimuro, Chem. Phys. Lett. 260 (1996) 147–152.
[16] H.A. Frank, J.A. Bautista, J. Josue, Z. Pendon, R.G. Hiller, F.P. Sharples, D. Gosztola, M.R. Wasielewski, J. Phys. Chem. B 104 (2000) 4569–4577.
[17] D. Zigmantas, T. Polivka, R.G. Hiller, A. Yartsev, V. Sundström, J. Phys. Chem. A 105 (2001) 10296–10306.
[18] H.M. Vaswani, C.P. Hsu, M. Head-Gordon, G.R. Fleming, J. Phys. Chem. B 107 (2003) 7940–7946.
[19] D. Zigmantas, R.G. Hiller, F.P. Sharples, H.A. Frank, V. Sundstrom, T. Polivka, Phys. Chem. Chem. Phys. 6 (2004) 3009–3016.
[20] V.S. Pavlovich, Biopolymers 82 (2006) 435–441.
[21] T. Polívka, V. Sundström, Chem. Rev. 104 (2004) 2021–2071.
[22] S. Shima, R.P. Ilagan, N. Gillespie, B.J. Sommer, R.G. Hiller, F.P. Sharples, H.A. Frank, R.R. Birge, J. Phys. Chem. A 107 (2003) 8052–8066.
[23] E. Papagiannakis, M. Vengris, D.S. Larsen, I.H.M. vanStokkum, R.G. Hiller, R. vanGrondelle, J. Phys. Chem. B 110 (2006) 512–521.
[24] T.A. Martinson, G.F. Plumley, Anal. Biochem. 228 (1995) 123.
[25] R.P. Ilagan, J.F. Koscielecki, R.G. Hiller, F.P. Sharples, G.N. Gibson, R.R. Birge, H.A. Frank, Biochemistry 45 (2006) 14052–14063.
[26] B.S. Hudson, B.E. Kohler, Synthetic Met. 9 (1984) 241–253.
[27] S. Liaaen-Jensen, in: G. Britton, S. Liaaen-Jensen, H. Pfander (Eds.), Carotenoids, Birkhäuser Verlag, Berlin, 1998, p. 217.
[28] T. Gillbro, R.J. Cogdell, Chem. Phys. Lett. 158 (1989) 312–316.
[29] Z.D. Pendon, G.N. Gibson, I. van der Hoef, J. Lugtenburg, H.A. Frank, J. Phys. Chem. B 109 (2005) 21172–21179.
[30] D.M. Niedzwiedzki, J.O. Sullivan, T. Polivka, R.R. Birge, H.A. Frank, J. Phys. Chem. B 110 (2006) 22872–22885.
[31] H.H. Billsten, D. Zigmantas, V. Sundström, T. Polívka, Chem. Phys. Lett. 355 (2002) 465–470.
[32] F.L. de Weerd, I.H.M. van Stokkum, R. van Grondelle, Chem. Phys. Lett. 354 (2002) 38–43.
[33] H. Cong, D.M. Niedzwiedzki, G.N. Gibson, H.A. Frank, J. Phys. Chem. 112 (2008) 3558–3567.
[34] I.H.M. van Stokkum, D.S. Larsen, R. van Grondelle, Biochim. Biophys. Acta 1657 (2004) 82–104.
[35] D. Niedzwiedzki, J.F. Koscielecki, H. Cong, J.O. Sullivan, G.N. Gibson, R.R. Birge, H.A. Frank, J. Phys. Chem. B 111 (2007) 5984–5998.
[36] B. DeCoster, R.L. Christensen, R. Gebhard, J. Lugtenburg, R. Farhoosh, H.A. Frank, Biochim. Biophys. Acta 1102 (1992) 107–114.
[37] T. Polívka, D. Zigmantas, H.A. Frank, J.A. Bautista, J.L. Herek, Y. Koyama, R. Fujii, V. Sundström, J. Phys. Chem. B 105 (2001) 1072–1080.
[38] D.A. Wild, K. Winkler, S. Stalke, K. Oum, T. Lenzer, Phys. Chem. Chem. Phys. 8 (2006) 2499–2505.
[39] M. Kopczynski, F. Ehlers, T. Lenzer, K. Oum, J. Phys. Chem. A 111 (2007) 5370–5381.
[40] F. Ehlers, D.A. Wild, T. Lenzer, K. Oum, J. Phys. Chem. A 111 (2007) 2257–2265.
[41] E.J. Larson, S.J. Pyszczynski, C.K. Johnson, J. Phys. Chem. A 105 (2001) 8136–8144.
[42] S. Yamaguchi, H.-o. Hamaguchi, J. Phys. Chem. A 104 (2000) 4272–4279.
[43] D.M. Niedzwiedzki, D.J. Sandberg, H. Cong, M.N. Sandberg, G.N. Gibson, R.R. Birge, H.A. Frank, Chem. Phys. (2008), in press, doi:10.1016/j.chemphys.2008.07.011.